An Electrochemical Cell for Operando Study of Lithium Batteries Using Synchrotron Radiation

J.B. Leriche, S. Hamelet, J. Shu, M. Morcrette, C. Masquelier, G. Ouvrard, M. Zerrouki, P. Soudan, S. Belin, E. Elkaïm, et al.

An Electrochemical Cell for *Operando* Study of Lithium Batteries Using Synchrotron Radiation

J. B. Leriche,[a] S. Hamelet,[a] J. Shu,[a] M. Morcrette,[a] C. Masquelier,[a,z] G. Ouvrard,[b] M. Zerrouki,[b] P. Soudan,[b] S. Belin,[c] E. Elkaïm,[c] and F. Baudelet[c]

[a]*Laboratoire de Réactivité et de Chimie des Solides, Université de Picardie Jules Verne, CNRS UMR 6007, 80039 Amiens Cedex 9, France*
[b]*Institut des Matériaux Jean Rouxel, Université de Nantes, CNRS UMR 6502, BP 32229, 44322 Nantes Cedex 3, France*
[c]*Synchrotron SOLEIL, L'Orme des Merisiers, Saint Aubin BP 48, 91192 Gif sur Yvette, France*

A new electrochemical cell has been specially designed for *operando* experiments at synchrotron facilities both for X-ray diffraction and X-ray absorption. It allows the investigation of insertion materials under high current densities (up to 5C rate) and hence to study complex phenomena of structural and electronic changes out of equilibrium. The $LiFePO_4$–$FePO_4$ system has been chosen as a case study to validate this cell, and tricky phenomena, with apparent delays in phase formation compared with the number of electrons exchanged, have been spotted.

The study of the structural and electronic evolution of lithium battery electrodes during charge/discharge processes is crucial to understand the Li storage/release mechanisms and to optimize these materials so as to achieve high performance and cyclability. To this end, in the past 20 years, several in situ and ex situ techniques, such as X-ray diffraction (XRD),[1-11] X-ray absorption spectroscopy (XAS),[12-15] and Mössbauer,[16] Raman, IR, and NMR [17,18] spectroscopies, have been developed.

In situ evaluation of battery materials, i.e., observation inside a closed electrochemical cell, brings online information and eliminates the risk of manipulating highly reactive powders with ambient atmosphere. It allows the investigation of complex reaction mechanisms and proves to account very satisfactorily for voltage–composition profiles in various chemical systems due to structural and electronic transitions within the electrode(s).

In situ XRD investigations can be performed both in standard laboratory diffractometers and synchrotron source facilities, the latter providing X-ray beams with a photon flux higher by several orders of magnitude than the ones delivered by conventional X-ray tubes. To this end, several kinds of electrochemical cells have been designed both for reflexion or transmission geometries. The recent development of high quality position sensitive detectors in standard X-ray diffractometers allows easier use of such techniques in laboratories. Quite universal in terms of materials to be investigated (crystalline and amorphous powders) and of phenomena to be described (structural changes and electronic transfer), in situ XAS experiments have been widely performed recently both in extended X-ray absorption fine structure (EXAFS) and X-ray absorption near edge structure (XANES) modes. For instance, although the EXAFS part of the signal provides direct structural information on the close environment of a given atom (selected by its own absorption energy), the XANES part of the spectrum can be roughly seen as a picture of the empty electronic states of a given atom and allows the monitoring of the filling of these levels (charge-transfer processes) during lithiation (and reverse). Recent approaches using band structure calculations and data simulation were very successful in allowing a precise analysis of chemical bonds during electrochemical lithium insertion/extraction.[19] Additionally, the development and use of bended single crystals in synchrotron facilities (dispersive X-ray absorption fine structure) and the possibility of fast rotation of the monochromator (QuickXAS) paved the way for new approaches for the study of battery materials at synchrotron facilities. The possibility of using very short acquisition times, typically on the order of a few seconds for both XRD and XAS, indeed permits us to investigate structural and electronic properties of electrodes out of equilibrium (contrary to standard in situ studies) at various current loadings, which we further refer to as the *operando* mode.

In this paper, we report on the development and use at the Synchrotron facility SOLEIL (France) of a new, reliable, and easy-to-use electrochemical cell designed for photon transmission or reflection geometry (both XRD and XAS) that allows fast (up to 5C, 850 mA g^{-1} of active material) and highly reversible electrochemical cycling. To perform experiments in different energy ranges, with various time and spatial resolutions, our goal, in the long term, is to use four different beamlines on the third-generation synchrotron source SOLEIL. These beamlines are CRISTAL for XRD, ligne utilisée pour la caractérisation par imagerie et absorption (LUCIA) for high spatial resolution and medium energy range XAS, spectroscopies applied to materials based on absorption (SAMBA) for classical and Quick XAS experiments at higher energy, and optique dispersive EXAFS for dispersive XAS (high time and spatial resolutions).[20] High rate $LiFePO_4$ powders are used as an illustrative example of positive electrode materials for Li-ion batteries to validate this cell working *operando* with synchrotron radiation.

Description of the Electrochemical Cell

One of the objectives of this study is to develop, so as to make it available to the scientific community, a user-friendly electrochemical cell to be used in synchrotron radiation facilities for both XRD and XAS experiments in transmission or reflection geometry. By user-friendly, we mean that the cell(s) should be mounted easily by the user in a standard Ar-filled glove box by stacking the positive electrode, the separator (soaked with electrolyte), and the negative electrode layer by layer in-between two XRD-transparent Be windows (the manipulation of which necessitates extreme care and knowledge of risks associated with its oxide, BeO). Additionally, it should be highly hermetic, stable in time, dismountable, reusable, easy to clean, easy to mount within the beamline, and easy to connect to the cycling potentiostat.

To this end, we extensively built and tested a stainless steel-based cell derived from the Swagelok configuration (Fig. 1).

1. The top part of the cell (used in most cases as the "positive" side of the cell vs metallic Li) is composed of a rigid, 5 cm large, outer ring with a hole (2 cm in diameter) behind which a metallic Be window (200 μm thick, 4 cm in diameter) is placed. This part is very similar to the cell already described in our recent papers[6,9] dealing with "standard" in situ XRD investigations within laboratory diffractometers using either Cu Kα or Co Kα radiations in reflection geometry. The electrode material to be investigated (either in powder, dried slurry, or plastic film form) may be placed directly behind the Be window, which acts as a metallic current collector

[z] E-mail: christian.masquelier@u-picardie.fr

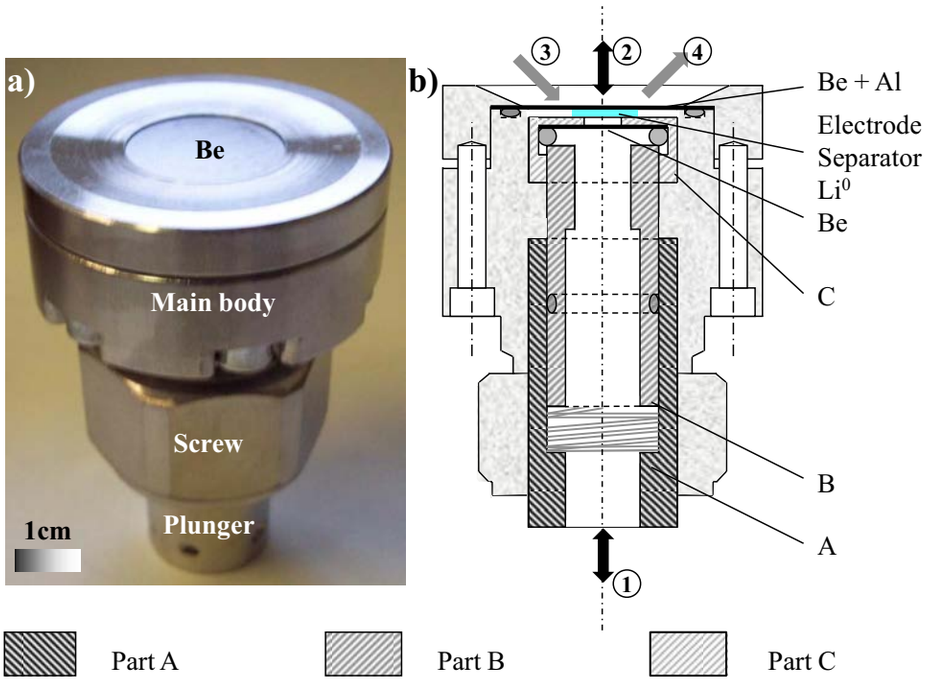

Figure 1. (Color online) Electrochemical cell for *operando* measurements. (a) Photo and (b) detailed view of the cell with incoming and outcoming beam paths in transmission geometry, and (c) incoming and (d) outcoming beam paths in reflexion geometry.

mostly transparent to X-rays (only 14.6% of the beam is absorbed at 5 keV and 0.71% at 20 keV). When positive electrode materials with operating voltages greater than 3.5 V vs Li are to be used, a thin (3–4 μm) aluminum foil is placed onto the Be window so as to protect it from oxidation. This part of the cell is then assembled to the main body with a rubber o-ring in contact with the Be window and through six stainless steel screws.

2. The second important piece of the cell (specially dedicated to transmission) is the cylindrical plunger (described in Fig. 1 as parts A, B, and C) that constitutes in most cases the "negative" part of the cell. As for the positive part, the plunger was designed so as to allow easy replacement of the Be window (200 μm thick, 2 cm in diameter in this case). Essential for the proper adjustment of the mechanical pressure within the cell, the two parts (A and B) of this plunger can translate along each other from the use of a spring. In transmission geometry, the incoming X-rays enter part A of the plunger (2 cm wide) through a cylindrical hole (1 cm wide, much larger than the beam size) and pass through the small Be window held with an o-ring between parts B and C. Part C is a capped cylinder with a rather small hole of 4 mm through which the beam goes before hitting the active part of the cell (Li/separator/positive electrode).

Electrochemical Tests

To validate this cell as a reliable tool for in situ/*operando* experiments at synchrotron facilities, we undertook, before any XRD or XAS experiment, a systematic electrochemical characterization of several positive electrode materials such as $LiMn_2O_4$, $LiFePO_4$, and $LiVPO_4F$, which operate between ~2.5 and 4.5 V vs Li.

The positive electrode materials, mixed with 10 wt % of carbon SP and poly(tetrafluoroethylene) binder, were deposited on 4 μm aluminum foil as plastic films for typically ~6 mg of active material/cm^2. Li metal was used as the counter (negative) electrode, and 1 M $LiPF_6$ in ethylene carbonate/diethyl carbonate (1:1, v/v) as the electrolyte impregnated in one layer of Whatman glass fiber or Celgard polymer was used as separators.

Electrochemical responses were recorded in a systematic way under several charge/discharge rates up to 5C (850 mA/g of active material, i.e., charge/discharge in 12 min) and demonstrated very good stability of the cell for at least 10 cycles, as shown for three representative voltage/composition data plotted in Fig. 2. Each experiment was repeated three to five times and showed very good reliability and reproducibility, essential for taking full advantage of allocated beam time at synchrotron facilities without worries for the electrochemistry part of the *operando* experiments.

Operando XRD on $LiFePO_4$-Based Powders

Triphylite $LiFePO_4$, a material of choice to be used as a positive electrode in the next generation of Li-ion batteries[21-26] particularly suited for applications in power tools and hybrid electric vehicles, was chosen as the first demonstrative example of the feasibility of

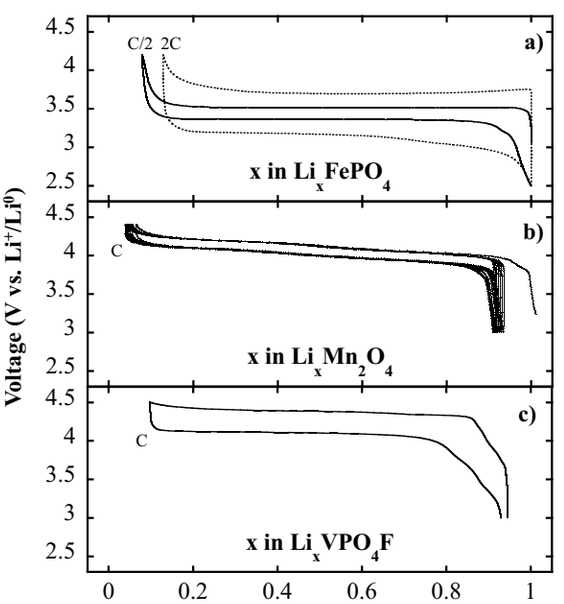

Figure 2. Electrochemical tests within the in situ cell of (a) $LiFePO_4$ (C/2 and 2C rates; 85 and 340 mA/g of active material), (b) $LiMn_2O_4$ (C rate; 148 mA/g), and (c) $LiVPO_4F$ (C rate; 155 mA/g).

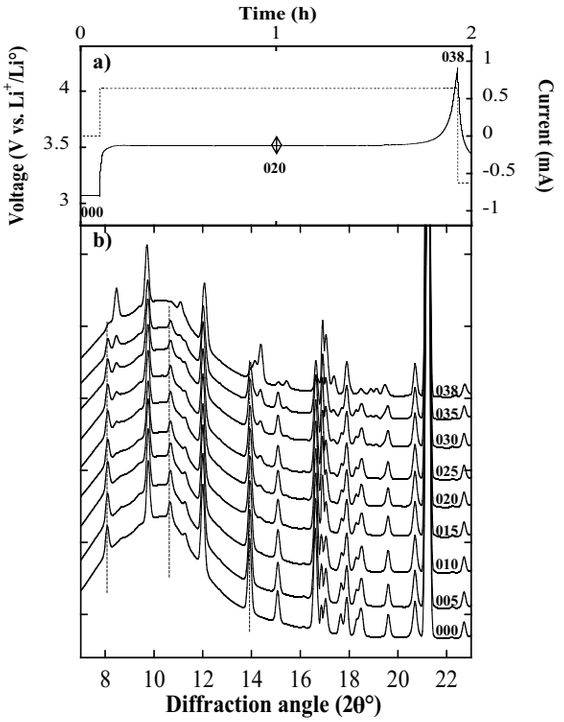

Figure 3. (a) Electrochemical data and (b) XRD patterns recorded *operando* during a charge at C/2 of $LiFePO_4$.

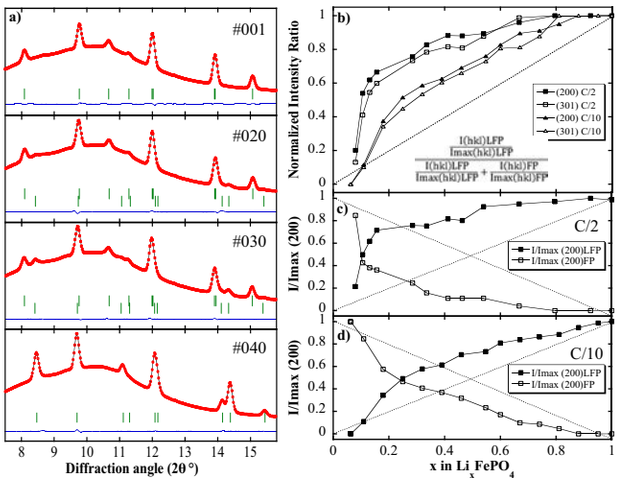

Figure 4. (Color online) XRD analysis of diffraction patterns obtained at C/2 and at C/10 during extraction of Li from $LiFePO_4$. (a) Full pattern matching refinements of C/2 data. [(b)–(d)] variations in normalized intensities as a function of x.

obtaining high quality XRD data in very short periods of time. We investigated several pristine powders of $LiFePO_4$ with different particle sizes, morphologies, and stoichiometry. The electrochemical cell was mounted for transmission geometry and connected to a galvanostat/potentiostat (VMP3 of Biologic). The incident X-ray wavelength chosen was 0.727 Å, allowing easy transmission through the many components of the cell, and the data were collected on an image plate detector, allowing very small recording times of 10 s per pattern. Altogether, seven batteries were cycled very reliably for an overall amount of ~2000 patterns recorded, from which the first series of interesting phenomena was spotted, as described below.

Figure 3 shows, for instance, the electrochemical and XRD data recorded *operando* during a charge lasting nearly 2 h during which 38 patterns were recorded (1 pattern of 10 s every 3 min). Classically described in the literature as a two-phase reaction between $LiFePO_4$ and $FePO_4$, the process of Li deintercalation appears to occur here with a significant delay; i.e., the diffractogram recorded at midcharge (20) is very far from being characteristic of a theoretical equal amount of both $LiFePO_4$ and $FePO_4$ phases. This apparent "crystallization delay" for the appearance of $FePO_4$ at the expense of the disappearance of $LiFePO_4$ was very recently observed by two other groups.[27-29] Chang et al.[27] interpreted their observations as the result of slow nucleation kinetics of the resulting phase, while process disturbances tend to stimulate the formation of nuclei. Chiang et al.[28,29] envisaged that the delay in the appearance of crystallized $FePO_4$ was due to the existence of transient intermediate amorphous $FePO_4$ components, the amount of which is dependent on (*i*) the particle size, (*ii*) the applied electrical overpotential, and (*iii*) the amplitude of the misfit strain between the lithiated and delithiated crystalline phases.

We carefully analyzed by full pattern matching refinements the variation in the intensities of several sets of diffraction peaks (several crystallographic directions) under two charge/discharge rates, i.e., within 2 h of charge (C/2; 85 mA/g of $LiFePO_4$) or 10 h (C/10; 17 mA/g of $LiFePO_4$). Much care was taken in selecting an appropriate background profile, in introducing anisotropic crystallite size parameters, and in normalizing the diffracted intensities vs the diffraction peak of Be used as a standard here. Figure 4a illustrates the quality of both the diffraction data and the refinements from which we were able to extract the variation in the normalized intensities of several sets of diffraction peaks of the two observed crystalline phases, i.e., $Li_{1-\varepsilon}FePO_4$ and $Li_{\varepsilon'}FePO_4$. Figure 4b illustrates, for instance, the decrease in the intensity of the $(200)_{Pnma}$ peak of $LiFePO_4$ as a function of x Li^+ overall content for both C/10 and C/2 rates. It shows a significant experimental deviation from the theoretical 50% decrease in intensity at midcharge (dotted line) more obvious at C/2 than at C/10. In an apparent contradiction with the recent interpretation of Chiang et al.,[28,29] the appearance of $(200)_{FePO_4}$ is also delayed but "grows" experimentally at the same rate as $(200)_{LiFePO_4}$ decreases (Fig. 4c). Indeed, the variations in the normalized intensities of both $Li_{1-\varepsilon}FePO_4$ and $Li_{\varepsilon'}FePO_4$ are somehow symmetrical and, as a consequence, cross each other at 50% of relative intensity for both phases. This observation suggests that, all over the charge process, only two crystalline phases are present, without the formation of a third amorphous component in the system. Figure 4d shows that this observed phenomenon is less pronounced at a C/10 rate. This prompted us to address porous electrode effects in more detail, which are under experimental investigation as of this date.

To get a deeper insight into this apparently new mechanism, we tried to precisely analyze the variation in the full width at half-maximum of the diffraction peaks (hence, the variation in crystallite sizes in several crystallographic directions), without success unfortunately, as the resolution of the diffracted pattern was not high enough (price to pay for fast acquisition with the image plate). This very important issue will be addressed very soon through a series of experiments designed for recording diffraction patterns with a higher instrumental resolution and a higher crystallinity of the $LiFePO_4$ powder.

Operando XAS on $LiFePO_4$-Based Powders

In addition to XRD, the technical development of our cell allowed us to investigate the local electronic and atomic structure of the $LiFePO_4$ electrodes at the thermodynamic equilibrium and during the charge and discharge process (*operando*) using in situ XAS at the Fe K edge. XAS data were collected in the transmission detection mode. The data reduction of the XAS spectra was performed using the software program ATHENA for Windows.[30] Stan-

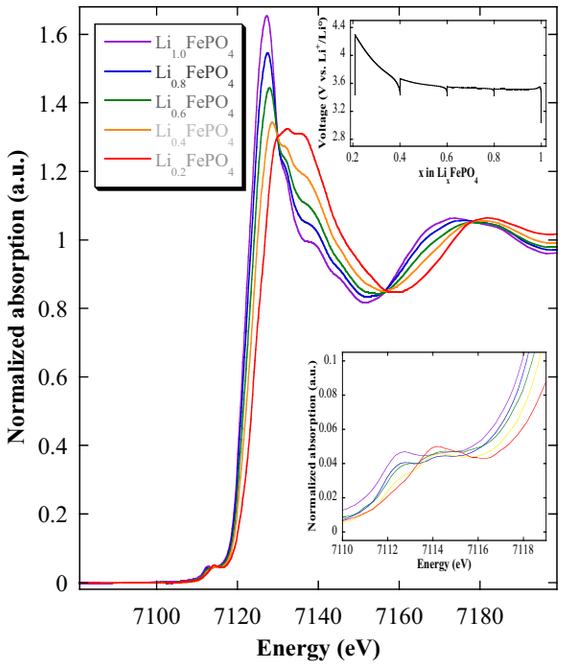

Figure 5. (Color online) Normalized absorption at the iron K edge (recorded at the equilibrium) for various states of charge within the $LiFePO_4/FePO_4$ system. The top insert is the corresponding charge curve, and the bottom insert is an expanded view of the pre-edge part.

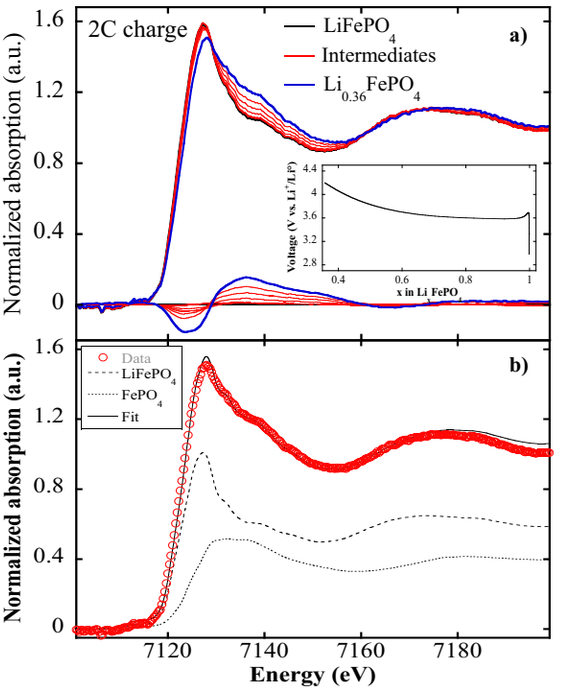

Figure 6. (Color online) (a) Normalized absorption at the iron K edge for various compositions in the $FePO_4/LiFePO_4$ system and (b) linear combination fit for the nominal $Li_{0.36}FePO_4$ composition.

dard procedures given in these programs were used to obtain the normalized and calibrated spectra.

The thermodynamic equilibrium study was carried out on the SAMBA beamline using a Si(111) double-crystal sagittal focusing monochromator. The size of the beam was 300 × 500 μm. The XAS measurements were recorded using three ionization chambers in a series to measure the intensities of the incident beam, the beam transmitted by the sample, and the beam transmitted by the Fe reference foil. For each $\Delta x = 0.2$ corresponding to the lithium ions extracted/inserted during charge/discharge, the electrode was stored at an open-circuit voltage for 30 min after which the XAS spectra were recorded (Fig. 5). For this experiment, a rate of 1C (170 mA/g of active material) was used (charging curve plotted in the insert of Fig. 5). The superposition of XAS spectra recorded at various states of charge displays clear isosbestic points showing a two-phase process at the spatial scale used. These results agree well with the literature.[12]

Within the XANES spectra, the edge positions shift progressively to higher energies during the charge process as a result of the oxidation of Fe^{2+} to Fe^{3+}.[31] As a consequence of the biphasic nature of the electrochemical process, each XANES spectrum is a linear combination of the $LiFePO_4$ and $FePO_4$ spectra with approximately the same percentage as in the electrochemical data. For example, the best linear combination fit for the $Li_{0.4}FePO_4$ composition (0.6 Li extracted) yields 37.4% of $LiFePO_4$ and 62.6% of $FePO_4$.

For dynamic studies, XANES data have been collected using a charge-coupled device camera on the ODE beamline dedicated to energy-dispersive XAS. In this setup, each spectrum is recorded during 10 s. Some spectra collected at different Li contents during charge at the 2C rate (340 mA/g of $LiFePO_4$) are gathered in Fig. 6a. As for the data recorded at equilibrium (Fig. 5), XANES spectra show isosbestic points confirming the biphasic character of the process with, again, an apparent delay during charge and discharge of the battery compared to the number of Li^+ extracted electrochemically. Indeed, during discharge/charge, each spectrum is a linear combination between $LiFePO_4$ and $FePO_4$ (taken at the equilibrium on the SAMBA beamline). Figure 6b shows the simulation done for a global composition of $Li_{0.36}FePO_4$ (0.64 Li^+ extracted) for which the best fit gives 61% of $LiFePO_4$ and 39% of $FePO_4$ (0.39 Li^+ extracted). The extraction process seems to occur with a delay with reference to the electrochemistry. This delay confirms our results obtained by XRD.

Conclusion

High quality XRD and XAS data can be obtained by using this in situ cell to reveal the complex nature of the transformation dynamics during the charge/discharge of electrodes for lithium-ion batteries. Such a cell allows the *operando* observation of these phenomena and will be used in the near future as a powerful tool to investigate possible inhomogeneities in porous electrodes.

Acknowledgment

We thank Professor Jean-Marie Tarascon and Dr. Charles Delacourt for fruitful discussions. The present work was undertaken within the ANR program Stock-E under the contract ANR-07-Stock-E-09-01. We also acknowledge the financial support of UMICORE (Belgium) for SH.

Centre National de la Recherche Scientifique assisted in meeting the publication costs of this article.

References

1. J. R. Dahn and R. R. Haering, *Solid State Commun.*, **40**, 245 (1981).
2. B. Gustafsson and J. Thomas, *Electrochim. Acta*, **37**, 1639 (1992).
3. J.-M. Tarascon, A.S. Gozdz, C. Schmutz, F. Shokoohi, and P. C. Warren, *Solid State Ionics*, **86/88**, 49 (1996).
4. S. Mukerjee, T. R. Thurston, N. M. Jisrawi, X. Q. Yang, J. McBreen, M. L. Daroux, and X. K. King, *J. Electrochem. Soc.*, **145**, 466 (1998).
5. T. R. Thurston, N. M. Jisrawi, S. Mukerjee, X. Q. Yang, J. McBreen, M. L. Daroux, and X. K. King, *Appl. Phys. Lett.*, **69**, 194 (1996).
6. M. Morcrette, Y. Chabre, G. Vaughan, G. Amatucci, J. B. Leriche, S. Patoux, C. Masquelier, and J. M. Tarascon, *Electrochim. Acta*, **47**, 3137 (2002).
7. M. Morcrette, J. B. Leriche, S. Patoux, C. Wurm, and C. Masquelier, *Electrochem. Solid-State Lett.*, **6**, A80 (2003).
8. S. Patoux, G. Rousse, J. B. Leriche, and C. Masquelier, *Chem. Mater.*, **15**, 2084 (2003).

9. A. S. Prakash, D. Larcher, M. Morcrette, M. S. Hegde, J.-B. Leriche, and C. Masquelier, *Chem. Mater.*, **17**, 4406 (2005).
10. K. Nikolowski, C. Baehtz, N. N. Bramnik, and H. Ehrenberg, *J. Appl. Crystallogr.*, **38**, 851 (2005).
11. C. Baehtz, T. Buhrmester, N. N. Bramnik, K. Nikolowski, and H. Ehrenberg, *Solid State Ionics*, **176**, 1647 (2005).
12. A. Deb, U. Bergman, E. J. Cairns, and S. P. Crameer, *J. Synchrotron Radiat.*, **11**, 497 (2004).
13. O. Haas, A. Deb, E. J. Cairns, and A. Wokaun, *J. Electrochem. Soc.*, **152**, A191 (2005).
14. I. Nakai, Y. Shiraishi, and F. Nishikawa, *Spectrochim. Acta, Part B*, **54**, 143 (1999).
15. I. Nakai and T. Nakagome, *Electrochem. Solid-State Lett.*, **1**, 259 (1998).
16. A. Ibarra-Palos, C. Darie, O. Proux, J. L. Hazemann, L. Aldon, J. C. Jumas, M. Morcrette, and P. Strobel, *Chem. Mater.*, **14**, 1166 (2002).
17. M. Letellier, F. Chevallier, C. Clinard, E. Frackowiak, J. N. Rouzaud, F. Beguin, M. Morcrette, and J. M. Tarascon, *J. Chem. Phys.*, **118**, 6038 (2003).
18. B. Key, R. Bhattacharyya, M. Morcrette, V. Seznec, J. M. Tarascon, and C. Grey, *J. Am. Chem. Soc.*, **131**, 9239 (2009).
19. F. Boucher, N. Bourgeon, K. Delbé, P. Moreau, D. Guyomard, and G. Ouvrard, *J. Phys. Chem. Solids*, **67**, 1238 (2006).
20. http://www.synchrotron-soleil.fr/portal/page/portal/Accueil, last accessed 2009.
21. A. K. Padhi, K. S. Nanjundaswamy, and J. B. Goodenough, *J. Electrochem. Soc.*, **144**, 1188 (1997).
22. J. B. Goodenough, A. K. Padhi, K. S. Nanjundaswamy, and C. Masquelier, World Pat. WO9740541 (1997).
23. N. Ravet, J. B. Goodenough, S. Besner, M. Simoneau, P. Hovington, and M. Armand, Abstract 127, The Electrochemical Society Meeting Abstracts, Vol. 99-2, Honolulu, HI, Oct 17–22, 1999.
24. M. Armand and J. M. Tarascon, *Nature (London)*, **451**, 652 (2008).
25. A. Yamada, S. C. Chung, and K. Hinokuna, *J. Electrochem. Soc.*, **148**, A224 (2001).
26. Y. M. Chiang, A. S. Gozdz, and A. W. Payne, U.S. Pat. US2007/0,031,732A1 (2007).
27. H. H. Chang, C. C. Chang, H. C. Wu, M. H. Yang, H. S. Sheu, and N. L. Wu, *Electrochem. Commun.*, **10**, 335 (2008).
28. M. Tang, H. Y. Huang, N. Meethong, Y. H. Kao, W. C. Carter, and Y. M. Chiang, *Chem. Mater.*, **21**, 1557 (2009).
29. Y. M. Chiang, in ICMAT Conference, Singapore, July 2009.
30. B. Ravel and M. Newville, *J. Synchrotron Radiat.*, **12**, 537 (2005).
31. J. L. Jones, J. T. Hung, and Y. S. Meng, *J. Power Sources*, **189**, 702 (2009).